# Direct observation of the Yb($4f^{13}6s^2$)F states and accurate determination of the YbF ionization energy

Thomas D. Persinger,[1] Jiande Han,[1] Anh T. Le,[2] Timothy C. Steimle,[3] and Michael C. Heaven[1,*]
[1]*Department of Chemistry, Emory University, Atlanta, Georgia 30322, USA*
[2]*School of Chemistry and Biochemistry, Georgia Institute of Technology, Atlanta, Georgia 30318, USA*
[3]*School of Molecular Sciences, Arizona State University, Tempe, Arizona 85287, USA*

(Received 2 August 2022; accepted 15 November 2022; published 2 December 2022)

YbF has been identified as a molecule that can be used to investigate charge-parity symmetry violations that are beyond the standard model of particle physics. Cooling to sub-milli-Kelvin is advantageous for experiments that probe manifestations of these symmetry violations. One approach involves laser cooling of YbF via the $A^2\Pi_{1/2}$–$X^2\Sigma^+$ transition. However, it appears that cooling by means of this transition may be limited by the radiative loss of population from the cooling cycle. YbF has low-energy states that arise from the $Yb^+(4f^{13}6s^2)F^-$ configuration. Recent theoretical calculations [C. Zhang *et al.*, J. Mol. Spectrosc. **386**, 111625 (2022)] predict that radiative decay from $A^2\Pi_{1/2}$ to the $4f^{13}6s^2$ states occurs with a branching fraction of approximately $10^{-3}$. In the present study we have used dispersed laser induced fluorescence spectroscopy to observe the lowest energy $4f^{13}6s^2$ states. These measurements were carried out using excitation of previously unobserved YbF transitions in the near UV spectral range. An accurate ionization energy (IE) of 48 703 ± 5 $cm^{-1}$ for YbF is also reported. A two-color photoionization technique was used to determine the IE and observe the $v^+ = 0$-3 vibrational levels of $YbF^+$ $X^1\Sigma^+$.

DOI: 10.1103/PhysRevA.106.062804

## I. INTRODUCTION

Here we present an experimental identification of the low-lying electronic state of YbF using dispersed laser induced fluorescence (DLIF), which has implications for photon cycling and laser cooling experiments. The heavy polar diatomic molecule YbF has received considerable attention over the past 25 years since it was first proposed as a venue for electric dipole moment (EDM) measurements [1–3]. It was noted early on [1] that the $^{174}$YbF isotopologue is well suited for determination of the leptonic sector electron EDM (eEDM, $d_e$), and that the $^{173}$YbF isotopologue can be used to investigate both $d_e$ and the nuclear magnetic quadrupole moment (MQM) of the $^{173}$Yb ($I = 5/2$) nucleus (hadronic sector). The MQM of the $^{173}$Yb nucleus arises from the composite effect of the EDM of the constituent nucleons, $d_N$, and the intranuclear $T$, $P$-odd forces (where $T$ and $P$ indicate time-reversal and discrete parity symmetries). The $T$, $P$-odd MQM interacts with the gradient of the magnetic field produced by the unpaired electron to produce a molecular EDM [4–6]. An EDM of an elementary particle (e.g., $d_e$ and $d_N$) violates both $T$ and $P$ symmetries. The standard model (SM) predicts that EDMs are exceptionally small [e.g., $d_e$ (SM) less than $10^{-38}$ $e$ cm] whereas theories beyond the standard model (BSM) frequently predict much larger values which in turn, due to the enhancement effect of the polar molecule, may produce a molecular EDM large enough to be measured by precision spectroscopy.

The two reported YbF-based attempted EDM measurements [7–9], both performed at Imperial College London, have focused on the determination of $d_e$. The goal is to observe the $d_e$-induced shift of the spacing of the $|N = 0, F = 1; M_F = +1\rangle$ and $|N = 0, F = 1; M_F = -1\rangle$ levels of the $X^2\Sigma^+(v = 0)$ vibronic states. The small $T$, $P$-odd energy shifts in YbF are determined by simultaneously subjecting the molecules to parallel electric and magnetic fields and using the measured spin-precession angular frequency [10,11] to determine the energy difference of states with opposite angular momentum projections. The $A^2\Pi_{1/2} - X^2\Sigma^+(0, 0)$ band is used for state preparation and detection. The uncertainty of the extracted estimate for $d_e$ is inversely proportional to the coherence time and, in the shot-noise limit, the square root of the photon counts of the $A^2\Pi_{1/2} - X^2\Sigma^+(0, 0)$ LIF signal used for detection [11]. The coherence time is dependent upon the flight time and divergence of a molecular beam of YbF as it travels through the parallel fields. The first YbF-based eEDM measurement [8] used a molecular beam produced by skimming the output of a high temperature effusive oven source and established an upper limit for $d_e$ of $(-0.2 \pm 3.2) \times 10^{-26}$ $e$ cm. The second reported YbF-based eEDM measurement attempt used a laser ablation supersonic expansion beam source and established an upper limit for $d_e$ of $(-2.4 \pm 5.7_{stat} \pm 1.5_{syst}) \times 10^{-28}$ $e$ cm [9].

A laser cooled sample could drastically improve the coherence time. One-dimensional [12] and two-dimensional [13] translational cooling of YbF has been recently demonstrated using a cryogenic buffer gas source and photon cycling of the $P_1(1)$ and $Q_{12}(1)$ lines of the $A^2\Pi_{1/2} - X^2\Sigma^+(0, 0)$ band for the main laser cooling transitions. Modeling the

*Corresponding author: mheaven@emory.edu

 

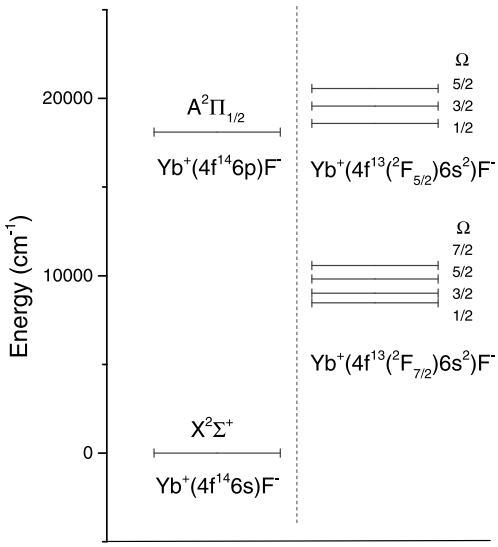


FIG. 1. Energy level diagram for YbF showing the electronic states of relevance to the present study.

two-dimensional (2D) cooling [13] suggested that there was a leak out of the cooling cycle to unobserved low-lying states having a dominant $Yb^+[4f^{13}(^2F_{7/2})6s^2]F^-$ configuration. These unobserved low-lying excited states had been used to explain the observed opposite sign [2] (relative to the alkaline earth monohalides) of the spin-rotation parameter $\gamma$ for the $X^2\Sigma^+(v=0)$ state, and the strong vibrational dependence of this parameter [14].

A nearly complete review of the previous spectroscopic investigations of YbF can be found in recent a deperturbation analysis [15]. That study addressed the nature of the well characterized $A^2\Pi_{1/2}$ $(v=0)$, [557], [561] states, and five other excited electronic states that have been observed at low spectral resolution. The results of relativistic electronic structure calculations for the $4f^{13}$ states and the strengths of transitions between these states and the $A^2\Pi_{1/2}$ $[Yb^+(4f^{14}6p^1)F^-]$ and $X^2\Sigma^+$ $[Yb^+(4f^{14}6s^1)F^-]$ states were also presented.

Figure 1 is a partial energy level diagram for YbF, showing the states that are relevant to the present study. The lowest energy $4f^{13}$ states are derived from the $Yb^+[4f^{13}(^2F_{7/2})6s^2]F^-$ configuration where, under the influence of the ligand field, the atomic ion $J_a=7/2$ state splits into molecular states with $\Omega=1/2$, 3/2, 5/2, and 7/2, where $\Omega$ is the unsigned projection of the electronic angular momentum along the interatomic axis. The higher energy excited states are derived from the $Yb^+[4f^{13}(^2F_{5/2})6s^2]F^-$ configuration, and the atomic ion $J_a=5/2$ state splits into molecular states with $\Omega=1/2$, 3/2, and 5/2. The energy interval between the $J_a=7/2$ and 5/2 manifolds is expected to be approximately 10 000 $cm^{-1}$ based upon the energies of the $^2F_{7/2}$ ($E=21\,418$ $cm^{-1}$) and $^2F_{5/2}$ ($E=31\,568$ $cm^{-1}$) states arising from the $[Xe]4f^{13}6s^2$ configuration of $Yb^+$. Electronic structure calculations, combined with the experimentally determined molecular constants and a deperturbation analysis [15], puts the three $J_a=5/2$ states in the range 18 000-21 000 $cm^{-1}$ and the five $J_a=5/2$ states in the range 8000-11 000 $cm^{-1}$. The nearly degenerate [561] ($E\sim561$ THz $=18\,713$ $cm^{-1}$) and [557] ($E\sim557$ THz $=18\,580$ $cm^{-1}$) states were assigned [15] as admixtures of $A^2\Pi_{1/2}$ $(v=1)$ and the $\Omega=1/2$ state of the $Yb^+[4f^{13}(^2F_{5/2})6s^2]F^-$ manifold (the THz labels are given to connect with previously published studies [14–16]).

Given this background, it is of interest to carry out experimental tests of the theoretical predictions. In the present study we have focused on determination of the energies of the $4f^{13}(^2F_{7/2})6s^2$ states. The strategy for these measurements was to observe transitions down to these states following laser excitation of suitable electronically excited states. The previously characterized $A^2\Pi$ and $B^2\Sigma^+$ states [14,17–19] were not considered viable upper state candidates as the transitions from these states to the $4f^{13}6s^2$ states were predicted [15] to be weak, and the long wavelengths of the emissions would not be compatible with the detectors available for this project. To circumvent these problems, we considered it likely that there would be higher energy states that would have mixed configurational parentage. This would permit both excitation from the ground state and emission back to the $4f^{13}6s^2$ states. A search for such states was made in the 31 000-33 500−$cm^{-1}$ range, as this would result in emissions down to the $4f^{13}(^2F_{7/2})6s^2$ states at wavelengths that could be detected using standard, high-gain photomultiplier tubes. As described in the following, this proved to be a successful approach.

The apparatus used for these measurements was also configured for accurate determinations of ionization energies (IEs), and the IE of YbF is a property of both thermodynamic significance and theoretical interest [20,21]. Uncertainty in the IE propagates through schemes where measurements of the bond dissociation energy for $YbF^+$ are used to assess the bond dissociation energy for the neutral molecule [20–25]. The previous best estimate [20,25] for the IE of YbF was $47\,700\pm400$ $cm^{-1}$. In the present work we have used resonant two-photon ionization techniques to obtain an accurate IE for YbF, and to determine the vibrational constants of $YbF^+$, $X^1\Sigma^+$.

## II. EXPERIMENT

The instrumentation used to record gas-phase spectra for YbF has been described previously [26]. YbF was obtained by pulsed 1064-nm Nd/YAG laser ablation of the surface of a Yb rod. The rod was mounted in a Smalley-type jet expansion source [27] where it was rotated and translated to avoid pitting. The carrier gas was a mixture of 0.5% $SF_6$ in He, supplied by a pulsed valve (Parker-Hannifin series 9) at a source pressure of 5 atm. Laser induced fluorescence (LIF) and dispersed laser induced fluorescence (DLIF) spectra were recorded with the excitation laser beam set to cross the jet expansion approximately 7.5 cm downstream from the nozzle orifice. LIF was collected along an axis that was perpendicular to both the laser beam axis and the jet expansion axis. For the recording of LIF data, a long-pass filter was used to reduce the scattered laser light, and the filtered fluorescence was detected by a photomultiplier tube (Photonis XP2020). DLIF spectra were obtained when the long-pass filter was replaced by a 0.25-m monochromator (Jarrell-Ash 82–410). With this instrument the line centers of the emission bands could be determined with an error range ($1\sigma$) of 10 $cm^{-1}$. In one series of measurements the 0.25-m monochromator was replaced by

a 0.64-m monochromator (ISA HR640) to reduce the error range to 2 $cm^{-1}$ for the lowest energy $4f^{13}6s^2$ state.

Two tunable dye laser systems were used in these experiments. These were Nd/YAG pumped systems, consisting of a Lambda Physik Scan Mate Pro driven by a Quantel Q-smart 850 Nd/YAG, and a Continuum ND6000 dye laser driven by a Powerlite 8000 Nd/YAG laser. The dye lasers operated with linewidths [full width at half maximum (FWHM)] of approximately 0.3 $cm^{-1}$. Frequency doubling of the output from the ND6000 dye laser was used to generate light in the 31 000-33 500−$cm^{-1}$ range.

Wavelength calibration of the dye lasers was established using a Bristol Instruments model 821 wave meter. The wavelength of the laser fundamental was measured to calibrate the frequency doubled light. Fluorescence decay curves were acquired using a digital oscilloscope (LeCroy WaveSurfer 24Xs) to signal average 256 laser pulses per trace. The 0.25-m monochromator was used to isolate the kinetics associated with specific, well-resolved emission lines.

Resonantly enhanced two-photon ionization (RE2PI), photoionization efficiency (PIE), and pulsed field ionization–zero kinetic energy electron (PFI-ZEKE) measurements were carried out in a differentially pumped vacuum chamber that was equipped for time-of-flight mass spectrometry and electron detection (our implementation of these techniques is described in detail in Ref. [26]). RE2PI and PIE spectra were recorded with mass-resolved cation detection. RE2PI data for transitions occurring in the near-UV spectral range were obtained using one-color, two-photon ionization. This was possible because the excited state energies were more than half of the IE. RE2PI spectra for lower energy states were observed using two-color ionization. All two-color measurements were carried out using spatially overlapped, counterpropagating laser beams. Digital delay generators (Stanford Research Systems, DG 535) were used to synchronize the light pulses.

PIE curves were recorded with the first laser set to populate an excited state of YbF. The wavelength of the second laser was then swept to locate the onset of ionization. These measurements were conducted with the ionization zone located between the charged electrodes of the mass spectrometer. The local electric field of 364 V $cm^{-1}$ caused a depression of the IE by 115 $cm^{-1}$ (this value is based on previous measurements where the field-free IE determined by PFI-ZEKE was compared to the IE obtained in the PIE measurements; for an example, see Ref. [28]). PFI-ZEKE spectra for $YbF^+$ were recorded with sequential laser excitation occurring under nominally field-free conditions. Sequential excitation to long-lived Rydberg states was followed by the application of a 1.4−V $cm^{-1}$ pulse to induce field ionization and acceleration of the electrons to a microchannel plate detector. The delay between the laser excitation and ionizing field pulses was 2 $\mu$s.

## III. RESULTS

The first step for this project was to locate electronically excited levels of YbF in the near-UV spectral range. The RE2PI technique was used for this search as the mass-resolved ion detection ensured that the carrier of the observed features would be YbF. Figures 2 and 3 show examples of intense transitions that were found in the target energy range. We did not attempt to rotationally resolve these features, but the band contour can be discerned in Fig. 2. The relatively sharp $Q$ branch, with a hint of blue shading, indicates that the rotational constant had increased slightly on electronic excitation. This change also results in a $P$-branch band head that is approximately 16 $cm^{-1}$ below the $Q$-branch maximum. Due to spectral congestion, it is more difficult to interpret the band contours of Fig. 3. For the present purpose, we note that the $Q$ branch of Fig. 2 (at 31 052 $cm^{-1}$) and the strong features at 32 800 and 33 058 $cm^{-1}$ of Fig. 3 (as indicated by arrows) were used in the recording of DLIF spectra.

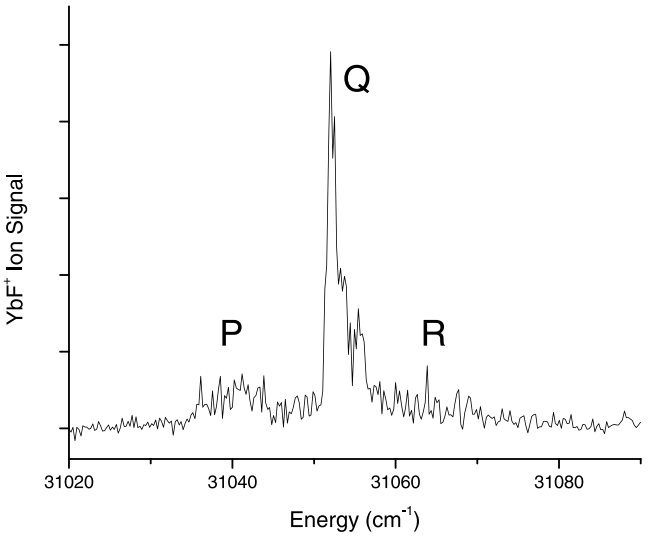


FIG. 2. One-color RE2PI spectrum of the YbF [31.05]1/2–$X^2\Sigma^+$ transition. This trace was recorded using detection of the $^{174}YbF^+$ isotopologue.

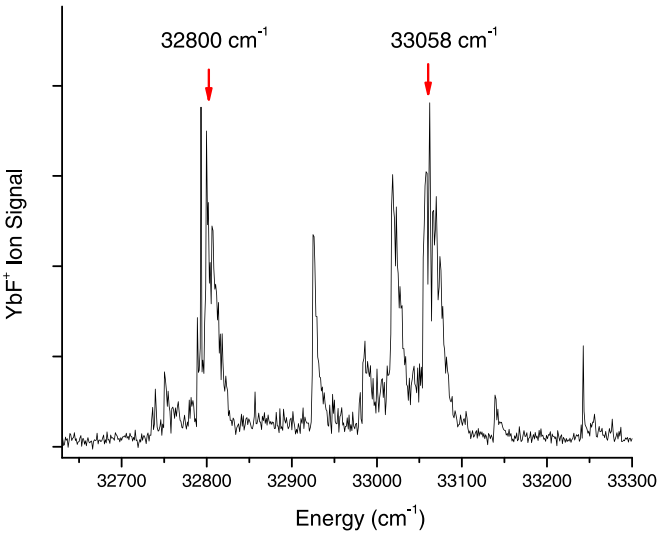


FIG. 3. One-color RE2PI spectrum of YbF showing the excitation features subsequently used in recording DLIF spectra. This trace was recorded using detection of the $^{174}YbF^+$ isotopologue.

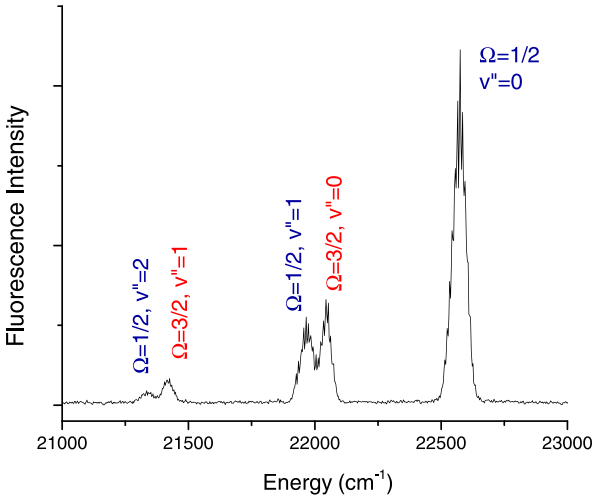


FIG. 4. DLIF spectrum obtained using excitation of the YbF [31.05]1/2–$X^2\Sigma^+$ transition at 31 052 $cm^{-1}$.

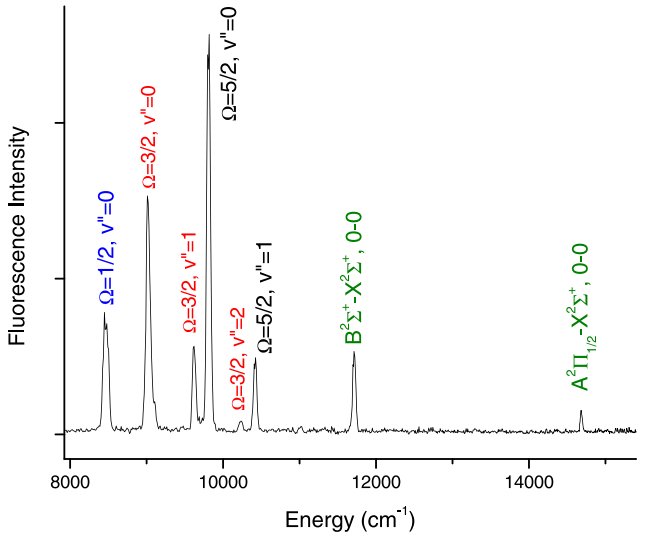


FIG. 5. DLIF spectrum obtained using excitation of the YbF [32.80]3/2–$X^2\Sigma^+$ transition at 32 800 $cm^{-1}$.

Figure 4 shows an expanded segment of the DLIF spectrum obtained by exciting the 31 052−$cm^{-1}$ band. The only other feature in this spectrum was a weak emission back to the ground state $v'' = 0$ level. This had an intensity that was approximately 1/10 of the strongest feature (without correction for the wavelength dependent sensitivity of the detection system). The lack of a vibrational progression for this emission suggests that the upper state is a $v' = 0$ vibrational level and that the equilibrium internuclear distance is close to that of the ground state. The emission bands shown in Fig. 4 were easily assigned using the $4f^{13}6s^2$ energy levels predicted by electronic structure calculations [29–31]. Transitions to the $\Omega'' = 1/2$ and 3/2 states were present, but emission down to $\Omega'' = 5/2$ levels were not observed. Based on the $\Delta\Omega = 0, \pm 1$ selection rule, we conclude that the upper state is $\Omega' = 1/2$. In the following, we label the UV excited states using the notation $[T_0/1000]\Omega$, where $T_0$ is the term energy in units of $cm^{-1}$. Hence, the upper state label for the band shown in Fig. 2 is [31.05]1/2.

Figure 5 shows the DLIF spectrum obtained by exciting the UV band at 32 800 $cm^{-1}$. The energy scale for this trace is the excitation energy minus the emission energy, giving the energy of the lower state relative to the ground state zero-point level. There are three interesting details of this spectrum. First, as was the case for Fig. 4, the emission back down to the ground state was weak (not shown). The second point of interest is that the most intense feature is the emission down to the $\Omega'' = 5/2, v'' = 0$ state, indicative of $\Omega' = 3/2$. Last, the lines at 11 721 and 14 689 $cm^{-1}$ do not originate from the initially excited level. They are the $B^2\Sigma^+$-$X^2\Sigma^+$ and $A^2\Pi_{1/2}$–$X^2\Sigma^+$ 0-0 transitions, where the upper states have been populated by radiative relaxation from [32.80] 3/2.

The DLIF spectrum obtained by exciting at 33 058 $cm^{-1}$ was dominated by transitions down to the $\Omega'' = 1/2$ and 3/2 states, indicating $\Omega' = 1/2$. The $B^2\Sigma^+$-$X^2\Sigma^+$ and $A^2\Pi$-$X^2\Sigma^+$ 0-0 emission bands were also present, but for the [33.06]1/2 upper state, the $A^2\Pi_{3/2}$ state was preferentially populated relative to $A^2\Pi_{1/2}$.

Energies for the $4f^{13}(^2F_{7/2})6s^2$ $\Omega'' = 1/2$, 3/2, and 5/2 states, derived from the DLIF spectra, are listed in Table I. Short vibrational progressions were observed, but the resolution was not sufficient for determination of the vibrational anharmonicity constants. The average vibrational intervals were 610, 607, and 610 ± 10 $cm^{-1}$ for $\Omega'' = 1/2$, 3/2, and 5/2, respectively. As transitions originating from the $4f^{13}(^2F_{7/2})6s^2$ $\Omega = 1/2$ $v = 0$ level might be used for repumping in laser cooling schemes, additional measurements were made to reduce the error range of the term energy for this state. DLIF spectra were recorded using the 0.64-m monochromator, with laser excitation at 30 800.3 ± 0.1 and 33 059.6 ± 0.1 $cm^{-1}$. The term energy ($T_0$) derived from these data was 8469 ± 2 $cm^{-1}$.

To examine the radiative decay kinetics of the UV excited states, we recorded fluorescence decay curves obtained by isolating emission features of interest. Figure 6 shows data obtained by monitoring the emissions from the [33.06]1/2, $B^2\Sigma^+$ $v' = 0$ and $A^2\Pi_{3/2}$ $v' = 0$ levels. Fitting a single exponential to the decay segment of the [33.06]1/2 state emission yielded a lifetime of 32 ± 5 ns. The temporal traces for the $B^2\Sigma^+$ and $A^2\Pi_{3/2}$ state emissions show maxima that occur later than the maximum of the [33.06]1/2 emission. The shift was consistent with the population of the $A^2\Pi_{3/2}$ and $B^2\Sigma^+$ states by radiative decay (the collision frequency in

TABLE I. Vibronic energies for the low-energy $Yb^+[4f^{13}(^2F_{7/2})6s^2]F^-$ states.

| $v$ | $\Omega = 1/2$ | $\Omega = 3/2$ | $\Omega = 5/2$ |
|---|---|---|---|
| 0 | 8469[a] | 9020 | 9810 |
| 1 | 9080 | 9630 | 10 420 |
| 2 | 9690 | 10 230 | |
| 3 | 10 300 | 10 840 | |

[a]Energies in $cm^{-1}$ units. The error range for the $\Omega = 1/2$ $v = 0$ level is ±2 $cm^{-1}$. All other error ranges are ±10 $cm^{-1}$.

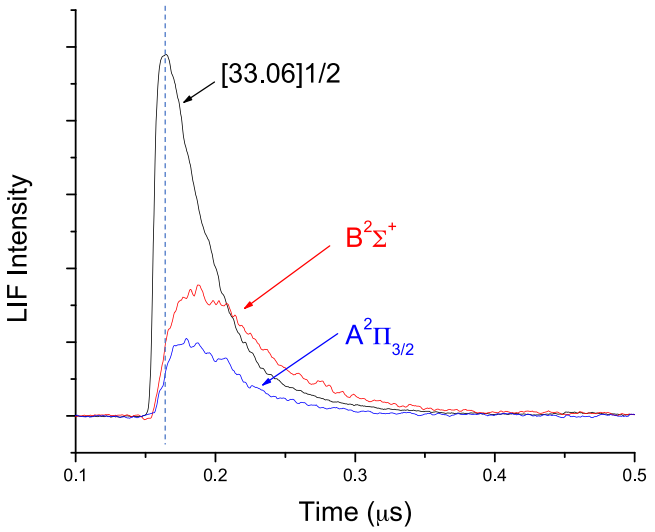


FIG. 6. Fluorescence decay curves recorded using excitation of the YbF[33.05]1/2–$X^2\Sigma^+$ transition at 33 058 $cm^{-1}$. The vertical dashed line indicates the time at which the UV emission reaches its maximum intensity.

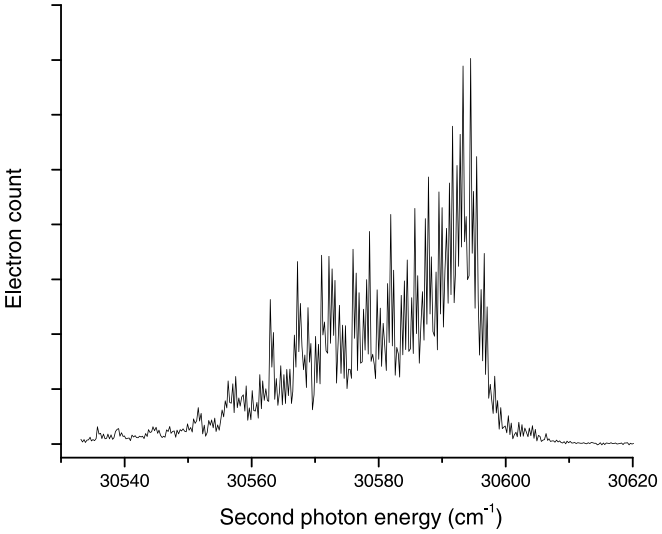


FIG. 7. PFI-ZEKE spectrum of the $YbF^+$ $X^1\Sigma^+$ origin band. The first photon was set to excite the YbF $A^2\Pi_{1/2}$–$X^2\Sigma^+$ 0-0 band at 18 106.3 $cm^{-1}$. The high-frequency oscillations of this trace were caused by shot-to-shot amplitude noise.

the downstream region of the jet expansion was far too low to contribute via nonradiative population transfer). Fitting a radiative cascade model to the temporal data for the $B^2\Sigma^+$ and $A^2\Pi_{3/2}$ states defined fluorescence decay lifetimes of $50 \pm 5$ and $35 \pm 5$ ns, respectively. The kinetic model was based on numerical integration of the coupled rate equations. The laser excitation step was simulated as a Gaussian temporal pulse with a duration of 10 ns (FWHM). Visual comparison of the experimental and simulated temporal curves was used to determine the optimal decay rates. These calculations were carried out using *Mathematica* 12. A lifetime for $A^2\Pi_{1/2}$ $v' = 0$ of $28 \pm 2$ ns was reported previously by Zhuang *et al.* [31].

Sequential two-photon ionization of YbF was examined using the $A^2\Pi_{1/2}$–$X^2\Sigma^+$ 0-0 band at 18 106.3 $cm^{-1}$ for the first excitation step. A preliminary value for the ionization threshold was then obtained by scanning the wavelength of the second laser over the range where the sum of the photon energies would cross the threshold for ionization (PIE scan). This process was monitored via the mass-resolved detection of $^{174}YbF^+$ ions. After correcting for the depression of the observed threshold due to the static electric field of the mass spectrometer, the threshold was found at $48\,700 \pm 20$ $cm^{-1}$.

The IE was refined by switching to the PFI-ZEKE technique, where ionization occurs under nominally field-free conditions. Figure 7 shows the PFI-ZEKE spectrum for ionization to the $YbF^+$ $X^1\Sigma^+$, $v^+ = 0$ level. The structure of this band is consistent with ionization from the range of rotational levels populated by the initial excitation of the $A^2\Pi_{1/2}$–$X^2\Sigma^+$ $Q$-branch maximum. The red-most edge of the band in Fig. 7 corresponds to ionization from the highest intermediate $J$ levels populated by the first laser pulse. As the energy of the second photon is increased, the ionization signal increases as lower $J$ levels are sequentially accessed. The cutoff on the blue side of the band occurs when the lowest energy $J$ level can be ionized. Hence, the blue edge from Fig. 7 was used to define an IE of $48\,703 \pm 5$ $cm^{-1}$. Scanning to higher energies revealed similar spectral features for the $v^+ = 1$, 2, and 3 levels. The energies of the $YbF^+$ states, relative to the YbF $X^2\Sigma^+$ $v'' = 0$ ground state, and $YbF^+$ $X^1\Sigma^+$ $v^+ = 0$, are listed in Table II. Fitting to the Morse expression for vibrational energies yielded constants of $\omega_e^+ = 604.9 \pm 1.1$ and $\omega_e x_e^+ = 2.7 \pm 0.3$ $cm^{-1}$.

## IV. DISCUSSION

Previous spectroscopic studies of YbF have examined transitions occurring at energies below 28 000 $cm^{-1}$, so the near UV transitions used in this study are reported. The DLIF spectra show short vibrational progressions with intensity envelopes indicating that the upper state vibrational levels are $v' = 0$, and that the molecular constants for the states are close to those of the low-energy $4f^{13}6s^2$ states.

Pototschnig *et al.* [30] used relativistic electronic structure calculations to predict states of YbF with term energies up to 25 023 $cm^{-1}$. Due to the large number of excited states, they were not able to assign the bands reported by Uttam and Joshi [32] for the 21 700-28000−$cm^{-1}$ spectral range. Given the complexity at even higher energies, we can only

TABLE II. Energies of the $YbF^+$ $X^1\Sigma^+$ vibrational states, relative to the zero-point levels of YbF $X^2\Sigma^+$ and $YbF^+$ $X^1\Sigma^+$.

| $v^+$ | $X^1\Sigma^+(cm^{-1})$[a]p | $T_0$ ($cm^{-1}$)[b] |
|---|---|---|
| 0 | 48 703.0 | 0 |
| 1 | 49 303.5 | 600.5 |
| 2 | 49 897.0 | 1194.0 |
| 3 | 50 489.8 | 1786.8 |

[a]The absolute energies are determined with errors of ±5 $cm^{-1}$.
[b]The energies relative to the origin band are determined with errors of ±1.5 $cm^{-1}$.

TABLE III. Comparison of observed and calculated energy levels for the low-energy $Yb^+(4f^{13}(^2F_{7/2})6s^2)F^-$ states.

| $\Omega$ | $T_0$ (exp) | $T_0$[a] | $T_0$[b] | $T_0$[c] |
|---|---|---|---|---|
| 1/2 | 8469 | 8607 | 9673 | 6146 |
| 3/2 | 9020 | 9113 | 10 224 | 6573 |
| 5/2 | 9810 | 9956 | 11 008 | 7164 |

Energies in $cm^{-1}$ units. With the exception of the $\Omega = 1/2$ state, which has measurement errors of $\pm 2$ $cm^{-1}$, the experimental energy errors are $\pm 10$ $cm^{-1}$.

[a]Zhang *et al.* (Ref. [15]), X2CAMF-EOM-CCSD calculations, empirically corrected.

[b]Pototschnig *et al.* (Ref. [30]), IHFS-CCSD, extrapolated to the complete basis set limit.

[c]Dolg *et al.* (Ref. [29]), relativistic multireference configuration interaction calculations.

provide a qualitative comment concerning the configurational parentage of the UV-excited states used in this work. The marked preference for emission back down to the $4f^{13}6s^2$ states and the fact that initial electronic excitation had a small effect on the bonding suggests that the atomic ion parentage contains a substantial contribution from $4f^{13}5d6s$ (see Fig. 2 of Ref. [30]).

A primary objective of the present study was to determine the energies of the low-energy $4f^{13}6s^2$ states, and use this information to evaluate the quality of the predictions made in the work of Zhang *et al.* [15]. The experimental results are compared to the predictions of high-level relativistic electronic structure calculations in Table III. Here it is apparent that the empirically adjusted calculations of Zhang *et al.* [15] yielded term energies that are close to the measured values (errors below 150 $cm^{-1}$). Good agreement was also achieved for the harmonic vibrational constants.

The computational techniques used by Zhang *et al.* [15] predicted the $4f^{14}6p$ and $4f^{13}6s^2$ states by means of single excitations from the ground state $4f^{14}6s$ configuration. The accuracy was not sufficient to capture the experimentally observed near degeneracy of the $A^2\Pi_{1/2}(v = 1)$ state with the $4f^{13}(^2F_{5/2})6s^2$ $\Omega = 1/2$ $(v = 0)$ state. The relative energies of the $4f^{13}(^2F_{5/2})6s^2$ and $4f^{13}(^2F_{7/2})6s^2$ manifold of states were fixed to the relativistic *ab initio* values. The absolute energies were empirically shifted to match the predicted energy (= 18 586 $cm^{-1}$) for the $4f^{13}(^2F_{5/2})6s^2$ $\Omega = 1/2$ $(v = 0)$ state that was obtained from the deperturbation analysis of the experimentally observed energies of the eight vibronic states mentioned above [15]. The agreement with the observed energy ordering and energy intervals for the $4f^{13}(^2F_{7/2})6s^2$ states strengthens the credibility of the transition moment calculations, which included values for the $A^2\Pi_{1/2}$–$X^2\Sigma^+$ vibronic bands that are critically important for the design of laser cooling schemes. Table III also contains previous theoretical results obtained using high-level, relativistic methods. The average differences between the calculated and observed energies of Pototschnig *et al.* [30] and Dolg *et al.* [29] were 1201 and 2472 $cm^{-1}$, respectively.

The previous best estimate [22–24,33] for the IE of YbF was 47 700 ± 400 $cm^{-1}$. The value measured by the PFI-ZEKE technique is higher by 1000 $cm^{-1}$. The probable reason for this discrepancy is that Kitaev *et al.* [24] used a high-temperature oven to generate gas phase YbF, combined with an electron impact technique to determine the IE. This approach often underestimates the IE as the observed ionization threshold is lowered by the presence of populations in thermally excited states [26]. The refined value for IE(YbF), combined with IE(Yb) = 50 443.2 $cm^{-1}$, shows that the bond dissociation energy of the ion is slightly greater than that of the neutral molecule [IE(Yb) − IE(YbF) = $D_0^+ - D_0 = 1740 \pm 5$ $cm^{-1}$]. This relatively small change in the dissociation energy is consistent with the removal of the marginally antibonding 6*s* electron. Pototschnig *et al.* [30] predicted the IE for YbF as a side issue in their theoretical study of the neutral molecule excited states. Their method used the closed-shell species $YbF^+$ and $YbF^-$ to generate sets of starting orbitals. Their best estimate for IE(YbF), obtained by extrapolation to the complete basis set limit, was 49 901 $cm^{-1}$.

Parker *et al.* [21] recently published a lower bound for the bond dissociation energy for $YbF^+$ of $D_0^+ > 43\,885$ $cm^{-1}$. With the new value for IE(YbF) this translates to a lower bound for the dissociation energy for neutral YbF of $D_0 >$ 42 145 $cm^{-1}$. This is larger than the estimate of 39 000 $cm^{-1}$ by Barrow and Chojnicki [17], but the difference is not surprising given that their estimate was based on a long extrapolation of spectroscopic data.

## V. SUMMARY

Dispersed laser induced fluorescence measurements have been used to examine the lowest energy states of YbF that correlate with the $Yb^+(4f^{13}(^2F_{7/2})6s^2)F^-$ electronic configuration. States with electronic angular momentum values of $\Omega'' = 1/2$, 3/2, and 5/2 were observed (these are Hund's case *c* states due to the strong spin-orbit coupling). The term energies for these states and their vibrational intervals were consistent with recent high-level computational predictions. Of particular interest, the experimental data support recent calculations that have been used to assess the potential for laser cooling of YbF via the $A^2\Pi_{1/2}$–$X^2\Sigma^+$ transitions. Zhang *et al.* [15] predicted that radiative decay from the $A^2\Pi_{1/2}$ $v' = 0$ level will populate the $4f^{13}(^2F_{7/2})6s^2$ $\Omega = 1/2$ state with a branching fraction of $5 \times 10^{-4}$. This factor is large enough that repump lasers may be needed to return the lost population back into the cooling cycle.

An accurate ionization energy for YbF was determined using the pulsed field ionization–zero kinetic energy photoelectron technique. The value obtained, 48 703 ± 5 $cm^{-1}$, was approximately 1000 $cm^{-1}$ higher than previous estimates. It is 1740 ± 5 $cm^{-1}$ below the IE for Yb, which indicates that the bond dissociation energy of the ion exceeds that of the neutral by the same amount. A vibrational progression was observed for $YbF^+$ $X^1\Sigma^+$, providing an experimental determination of the vibrational constants for the ion.

## ACKNOWLEDGMENTS

This work was supported by the National Science Foundation under Grant No. CHE-2055579. We thank Prof. L. Cheng (Johns Hopkins University) for his advice concerning the

previous electronic structure calculations for YbF, and Dr. M. R. Tarbutt (Imperial College, London) for helpful discussion concerning the laser cooling of YbF. We also thank Prof. R. W. Field (MIT) for his detailed critique of the paper and insights concerning ligand field theory, and P. Yu (PMA, Caltech) for his comments and suggestions.

[1] M. G. Kozlov and V. F. Ezhov, Phys. Rev. A **49**, 4502 (1994).
[2] B. E. Sauer, J. Wang, and E. A. Hinds, Phys. Rev. Lett. **74**, 1554 (1995).
[3] A. V. Titov, N. S. Mosyagin, and V. F. Ezhov, Phys. Rev. Lett. **77**, 5346 (1996).
[4] M. Denis, Y. Hao, E. Eliav, N. R. Hutzler, M. K. Nayak, R. G. E. Timmermans, and A. Borschesvky, J. Chem. Phys. **152**, 084303 (2020).
[5] V. V. Flambaum, D. DeMille, and M. G. Kozlov, Phys. Rev. Lett. **113**, 103003 (2014).
[6] M. S. Safronova, D. Budker, D. DeMille, D. F. J. Kimball, A. Derevianko, and C. W. Clark, Rev. Mod. Phys. **90**, 025008 (2018).
[7] J. J. Hudson, D. M. Kara, I. J. Smallman, B. E. Sauer, M. R. Tarbutt, and E. A. Hinds, Nature (London) **473**, 493 (2011).
[8] J. J. Hudson, B. E. Sauer, M. R. Tarbutt, and E. A. Hinds, Phys. Rev. Lett. **89**, 023003 (2002).
[9] D. M. Kara, I. J. Smallman, J. J. Hudson, B. E. Sauer, M. R. Tarbutt, and E. A. Hinds, New J. Phys. **14**, 103051 (2012).
[10] W. B. Cairncross and J. Ye, Nat. Rev. Phys. **1**, 510 (2019).
[11] C. J. Ho, J. A. Devlin, I. M. Rabey, P. Yzombard, J. Lim, S. C. Wright, N. J. Fitch, E. A. Hinds, M. R. Tarbutt, and B. E. Sauer, New J. Phys. **22**, 053031 (2020).
[12] J. Lim, J. R. Almond, M. A. Trigatzis, J. A. Devlin, N. J. Fitch, B. E. Sauer, M. R. Tarbutt, and E. A. Hinds, Phys. Rev. Lett. **120**, 123201 (2018).
[13] X. Alauze, J. Lim, M. A. Trigatzis, S. Swarbrick, N. J. Fitch, B. E. Sauer, and M. R. Tarbutt, Quantum Sci. Technol. **6**, 044005 (2021).
[14] J. Lim, J. R. Almond, M. R. Tarbutt, D. T. Nguyen, and T. C. Steimle, J. Mol. Spectrosc. **338**, 81 (2017).
[15] C. Zhang, C. Zhang, L. Cheng, T. C. Steimle, and M. R. Tarbutt, J. Mol. Spectrosc. **386**, 111625 (2022).
[16] I. J. Smallman, F. Wang, T. C. Steimle, M. R. Tarbutt, and E. A. Hinds, J. Mol. Spectrosc. **300**, 3 (2014).
[17] R. F. Barrow and A. H. Chojnicki, J. Chem. Soc., Faraday Trans. 2 **71**, 728 (1975).
[18] K. L. Dunfield, C. Linton, T. E. Clarke, J. McBride, A. G. Adam, and J. R. D. Peers, J. Mol. Spectrosc. **174**, 433 (1995).
[19] H. U. Lee and R. N. Zare, J. Mol. Spectrosc. **64**, 233 (1977).
[20] J. K. Gibson, J. Phys. Chem. A **126**, 272 (2022).
[21] M. L. Parker, J. Jian, and J. K. Gibson, Phys. Chem. Chem. Phys. **23**, 11314 (2021).
[22] V. N. Belyaev, N. L. Lebedeva, and K. S. Krasnov, Zh. Fiz. Khim. **70**, 1429 (1996).
[23] A. D. Chervonnyi and N. A. Chervonnaya, Zh. Neorg. Khim. **52**, 1314 (2007).
[24] A. A. Kitaev, I. S. Gotkis, P. G. Val'kov, and K. S. Krasnov, Izv. Vyssh. Uchebn. Zaved., Khim. Khim. Tekhnol. **31**, 56 (1988).
[25] A. L. Kaledin, M. C. Heaven, R. W. Field, and L. A. Kaledin, J. Mol. Spectrosc. **179**, 310 (1996).
[26] M. C. Heaven, Phys. Chem. Chem. Phys. **8**, 4497 (2006).
[27] M. A. Duncan, Rev. Sci. Instrum. **83**, 041101 (2012).
[28] T. D. Persinger, J. Han, and M. C. Heaven, J. Phys. Chem. A **125**, 3653 (2021).
[29] M. Dolg, H. Stoll, and H. Preuss, Chem. Phys. **165**, 21 (1992).
[30] J. V. Pototschnig, K. G. Dyall, L. Visscher, and A. S. P. Gomes, Phys. Chem. Chem. Phys. **23**, 22330 (2021).
[31] X. Zhuang, A. Le, T. C. Steimle, N. E. Bulleid, I. J. Smallman, R. J. Hendricks, S. M. Skoff, J. J. Hudson, B. E. Sauer, E. A. Hinds *et al.*, Phys. Chem. Chem. Phys. **13**, 19013 (2011).
[32] K. N. Uttam and M. M. Joshi, J. Mol. Spectrosc. **174**, 290 (1995).
[33] L. A. Kaledin, M. C. Heaven, and R. W. Field, J. Mol. Spectrosc. **193**, 285 (1999).